

Polariton relaxation under vibrational strong coupling: Comparing cavity molecular dynamics simulations against Fermi's golden rule rate

Tao E. Li,^{1, a)} Abraham Nitzan,^{1, 2, b)} and Joseph E. Subotnik^{1, c)}

¹⁾*Department of Chemistry, University of Pennsylvania, Philadelphia, Pennsylvania 19104, USA*

²⁾*School of Chemistry, Tel Aviv University, Tel Aviv 69978, Israel*

Under vibrational strong coupling (VSC), the formation of molecular polaritons may significantly modify the photo-induced or thermal properties of molecules. In an effort to understand these intriguing modifications, both experimental and theoretical studies have focused on the ultrafast dynamics of vibrational polaritons. Here, following our recent work [J. Chem. Phys., **154**, 094124, (2021)], we systematically study the mechanism of polariton relaxation for liquid CO₂ under a weak external pumping. Classical cavity molecular dynamics (CavMD) simulations show that polariton relaxation results from the combined effects of (i) cavity loss through the photonic component and (ii) dephasing of the bright-mode component to vibrational dark modes as mediated by intermolecular interactions. The latter polaritonic dephasing rate is proportional to the product of the weight of the bright mode in the polariton wave function and the spectral overlap between the polariton and dark modes. Both these factors are sensitive to parameters such as the Rabi splitting and cavity mode detuning. Compared with a Fermi's golden rule calculation based on a tight-binding harmonic model, CavMD yields similar parameter dependence for the upper polariton relaxation lifetime but sometimes a modest disagreement for the lower polariton. We suggest that this disagreement results from polariton-enhanced molecular nonlinear absorption due to molecular anharmonicity, which is not included in our analytical model. We also summarize recent progress on probing nonreactive VSC dynamics with CavMD.

I. INTRODUCTION

Strong light-matter interactions provide a novel approach towards modifying molecular properties by forming hybrid light-matter states — known as polaritons^{1–8}. In the past decade, vibrational strong coupling (VSC) was experimentally observed when a large number of molecules in the condensed phase were placed in a Fabry–Pérot microcavity and a vibrational mode of molecules formed strong coupling with a cavity mode^{9–12}. Under VSC, one of the most intriguing experimental observations is the possibility of modifying thermally activated ground-state chemical reactions through such a Fabry–Pérot microcavity and without a direct external pumping¹³. Inspired by this seminal observation¹³ from the Ebbesen group, intensive experimental and theoretical efforts have now been made to understand VSC-related chemistry. From an experimental point of view, there has been an extensive exploration of VSC catalytic effects in different types of chemical reactions^{14–20} and the use of VSC to alter other molecular properties in the absence of an external laser pumping²¹ has also been investigated; at the same time, spectroscopists have also focused on the ultrafast dynamics of vibrational polaritons by pump-probe^{22,23} and two-dimensional infrared (IR)^{24–29} spectroscopies. From a theoretical point of view, while the detailed mechanism of "VSC catalysis" is still not well understood^{30–38}, the current models of ultrafast polariton dynamics appear to be largely consistent with observations^{39–45}.

As far as the ultrafast dynamics of vibrational polaritons are concerned, recent experiments^{22–28} have emphasized the complicated interaction between polaritons and vibrational dark modes after the polariton pumping with an external laser field; see Ref.⁷ for a recent review. Two of the most nontrivial observations include (i) polariton mediated intermolecular vibrational energy transfer between two molecular species after the upper polariton (UP) pumping²⁷ and (ii) polariton enhanced molecular nonlinear absorption after the lower polariton (LP) pumping^{7,26}. While there have been a few theory papers on polariton relaxation based on analytic models^{39,42,46,47} and realistic modeling^{48–51}, a systematic study of vibrational polariton relaxation when realistic molecules are considered is still unavailable, which will be the focus of this paper.

Our approach for studying polariton relaxation is classical cavity molecular dynamics (CavMD) simulations^{45,52–54}, in which both the cavity modes and molecular vibrations are treated classically and move along an electronic ground state surface. Compared with standard theories for strong light-matter interactions, CavMD has two advantages: the ability to (i) describe realistic molecules and (ii) treat a very large number of molecules coupled to the cavity with an affordable computational cost. These advantages allow CavMD to identify nontrivial VSC effects beyond, e.g., the Tavis–Cummings Hamiltonian^{55,56} or the coupled oscillator model^{57,58}. The latter is necessary because, to date, most VSC experiments were performed with Fabry–Pérot cavities, in which the cavity volume is $\sim \lambda^3$ (where λ denotes the wavelength of the cavity mode) and the corresponding molecular number is very large (say, $N \sim 10^{10}$).

We note that recent considerations of the role of VSC played by symmetry and selection rules can in princi-

^{a)}Electronic mail: taoli@sas.upenn.edu

^{b)}Electronic mail: anitzan@sas.upenn.edu

^{c)}Electronic mail: subotnik@sas.upenn.edu

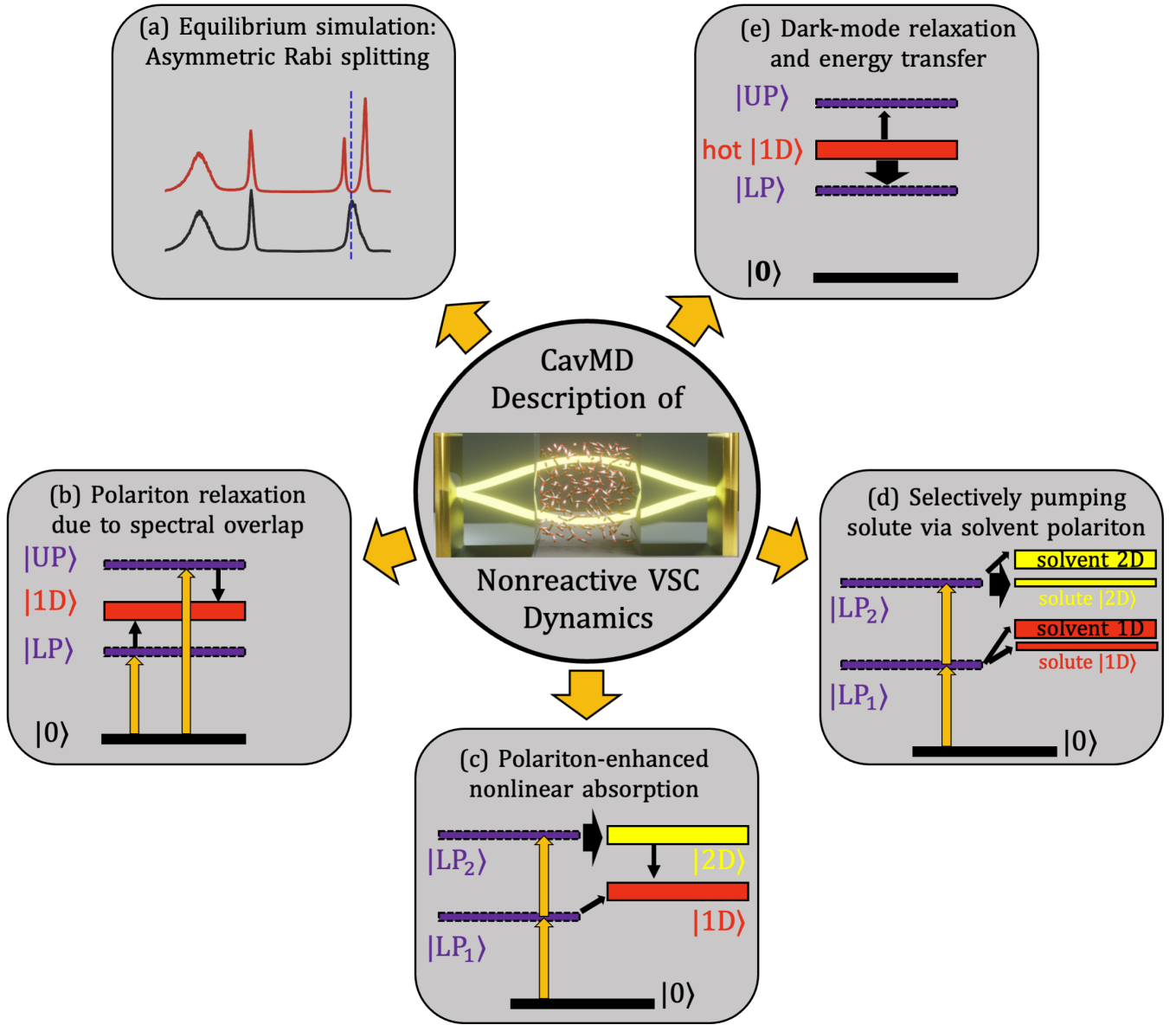


FIG. 1. Illustration of nonreactive VSC dynamics probed by CavMD simulations. (a) Asymmetric Rabi splitting under thermal equilibrium⁵². (b) Polariton relaxation to dark modes (this work). (c) Polariton-enhanced molecular nonlinear absorption⁴⁵. (d) Selectively exciting solute molecules via solvent polariton pumping⁵⁴. (e) Dark-mode relaxation and energy transfer dynamics⁵³. The cartoon in the middle circle demonstrates the simulation setup of CavMD, which is adapted from Ref.⁴⁵. See text around for details.

ple be studied by CavMD. However, we do not address these issues here. We also emphasize that CavMD is a classical approximation, so this approach may fail if any quantum effect (either from the nuclei or cavity photons) dominates the VSC effect (which is largely unexplored). In order to understand the applicability of CavMD, it is necessary to benchmark the performance of CavMD under various situations against experiments or analytic models; see the next paragraph and also Fig. 1 for a summary. Following the method in Ref.⁴⁵, here we will focus on using CavMD to describe polariton relaxation when the polariton is weakly pumped by an external laser field. In the weak pumping limit (which is also the con-

dition for most ultrafast experiments), we will compare the CavMD results with a quantum model where the polariton relaxation lifetime can be calculated by a Fermi's golden rule (FGR) rate. Together with an extensive parameter dependence study of polariton relaxation, this comparison will not only serve as an important performance benchmark of CavMD, but also facilitate a mechanistic understanding of vibrational polariton relaxation.

Before focusing on the details of vibrational polariton relaxation, as shown in Fig. 1, let us summarize some of the most important observations by CavMD from a series of recent publications (including this work) as well as the connection to different experiments and theories.

- (a) Asymmetric Rabi splitting from equilibrium CavMD simulations⁵². Since the self-dipole term is included in CavMD, this approach preserves gauge invariance^{59–61}. A direct consequence of including the self-dipole term is the asymmetry of the Rabi splitting even when the cavity mode is at resonance with the vibrational mode. For the linear IR spectrum of liquid water under VSC, CavMD not only yields similar results as the coupled oscillator model, but also shows that the polaritonic lineshape is much smaller than the inhomogeneous broadening of the water O–H peak. This result — which cannot be obtained from the coupled oscillator model — agrees with an early theoretical prediction⁶² and experimental observations in liquid water VSC¹⁴. This simulation also suggests that individual molecular properties are not meaningfully modified under VSC when thermal equilibrium is considered, suggesting a nonequilibrium or quantum origin of "VSC catalysis".
- (b) Mechanism of vibrational polariton relaxation (this work). Here, we will demonstrate that, for the UP, CavMD predicts a similar parameter dependence for the UP lifetime as does a FGR rate calculation based on a tight-binding harmonic model. We also highlight the significance of the dephasing process from the polariton to the dark modes due to the spectral overlap between the polariton and dark modes; this overlap can be controlled by the Rabi splitting and cavity mode detuning.
- (c) Polariton enhanced molecular nonlinear absorption⁴⁵. When twice the LP roughly matches the vibrational $0 \rightarrow 2$ transition (due to molecular anharmonicity), CavMD shows that strongly exciting the LP can directly transfer energy to the second ($|2D\rangle$) or higher excited states of vibrational dark modes; at later times, this excess energy gradually transfers to the first excited state of vibrational dark modes ($|1D\rangle$). The delayed excitation of $|1D\rangle$ states after the LP pumping has been experimentally reported previously²⁶ and a direct observation of the initial pumping of $|2D\rangle$ states has also been shown recently⁷. These experimental observations, together with a quantum model study⁴⁴, appear to validate our simulation results.
- (d) Selectively exciting solute molecules via solvent polariton pumping⁵⁴. Given the validity of the polariton enhanced molecular nonlinear absorption mechanism, CavMD shows that, if the LP of the solvent molecules can support the nonlinear transition of the solute (not the solvent) molecules only (i.e., twice the solvent LP roughly matches the solute $0 \rightarrow 2$ vibrational transition), pumping the solvent LP may highly excite the solute molecules, leaving the solvent molecules barely excited. This finding deserves experimental exploration in the near future.

- (e) Nonequilibrium dark-mode dynamics⁵³. For a small fraction of hot CO₂ molecules immersed inside a CO₂ thermal bath, in the absence of external pumping, the LP can be transiently excited even when the molecular system size is large. The transiently excited LP can accelerate vibrational relaxation of the hot molecules and promote the energy transfer to the thermal molecules. For small-volume cavities ($N < 10^4$), the VSC effect on the relaxation rate per molecule resonantly depends on the cavity mode frequency; for cavities with larger volumes, the VSC effect per molecule vanishes, despite the fact that the transiently excited LP prefers to transfer energy to the molecules at the tail of the energy distribution (which may connect to VSC catalytic effect). The vanished VSC effect (per molecule) on the dark-mode relaxation rate in a large volume cavity is consistent with a recent experiment with Fabry–Pérot cavities.²⁸

We now turn to (b) above and in the rest of this paper focus on investigating the mechanism of vibrational polariton relaxation. This paper is organized as follows. In Sec. II, we introduce the FGR calculation and CavMD simulations that we will employ in order to describe the polariton relaxation lifetime. In Sec. III we present results. We conclude in Sec. IV.

II. METHODS

A. Model system and the FGR rate

The standard theory for describing strong light-matter interactions in the collective regime is the Tavis–Cummings (TC) Hamiltonian^{55,56}. In this model, a single cavity mode with frequency ω_c is coupled to N identical two-level systems with transition frequency ω_0 :

$$\hat{H} = \hbar\omega_c \hat{a}^\dagger \hat{a} + \hbar\omega_0 \sum_{n=1}^N \hat{\sigma}_+^{(n)} \hat{\sigma}_-^{(n)} + \hbar g_0 \sum_{n=1}^N \left(\hat{a}^\dagger \hat{\sigma}_-^{(n)} + \hat{a} \hat{\sigma}_+^{(n)} \right). \quad (1)$$

Here, \hat{a}^\dagger and \hat{a} denote the creation and annihilation operators for the cavity photon; $\hat{\sigma}_+^{(n)} \equiv |ne\rangle \langle ng|$ and $\hat{\sigma}_-^{(n)} \equiv |ng\rangle \langle ne|$, where $|ng\rangle$ and $|ne\rangle$ denote the ground and excited state for the n -th two-level system; g_0 denotes the coupling constant between the cavity photon and each two-level system. In the light-matter coupling term (the last term above), both the long-wave approximation and the rotating-wave approximation have been taken.

For VSC, since high-frequency molecular vibrations can be approximated as harmonic oscillators at and below room temperature, we replace the two-level systems in Eq. (1) by quantum harmonic oscillators (with the creation and annihilation operators denoted by \hat{b}_n^\dagger and

\hat{b}_n) and obtain the following Hamiltonian:

$$\hat{H} = \hbar\omega_c \hat{a}^\dagger \hat{a} + \hbar\omega_0 \sum_{n=1}^N \hat{b}_n^\dagger \hat{b}_n + \hbar g_0 \sum_{n=1}^N \left(\hat{a}^\dagger \hat{b}_n + \hat{a} \hat{b}_n^\dagger \right). \quad (2)$$

This model Hamiltonian serves as the starting point of our derivation.

In the light-matter coupling term of Eq. (2), since the cavity photon interacts with a symmetric combination of the molecular operators only, one can introduce the bright-mode creation and annihilation operators as follows:

$$\begin{aligned} \hat{B} &= \frac{1}{\sqrt{N}} \sum_{i=1}^N \hat{b}_i, \\ \hat{B}^\dagger &= \frac{1}{\sqrt{N}} \sum_{i=1}^N \hat{b}_i^\dagger. \end{aligned} \quad (3)$$

All the other $N - 1$ linear combinations of the molecular operators are decoupled from the cavity mode and are called the dark modes:

$$\begin{aligned} \hat{D}_\mu &= \frac{1}{\sqrt{N}} \sum_{i=1}^N e^{i2\pi\mu/N} \hat{b}_i, \\ \hat{D}_\mu^\dagger &= \frac{1}{\sqrt{N}} \sum_{i=1}^N e^{i2\pi\mu/N} \hat{b}_i^\dagger. \end{aligned} \quad (4)$$

Here, $\mu = 1, 2, \dots, N - 1$ indexes the dark modes.

With the separation of bright and dark modes, the Hamiltonian in Eq. (2) becomes

$$\hat{H} = \hbar\omega_c \hat{a}^\dagger \hat{a} + \hbar\omega_0 \hat{B}^\dagger \hat{B} + \frac{1}{2} \hbar\Omega_N \left(\hat{a}^\dagger \hat{B} + \hat{a} \hat{B}^\dagger \right) + \hat{H}_D, \quad (5)$$

where $\Omega_N \equiv 2\sqrt{N}g_0$ and \hat{H}_D is the Hamiltonian for the dark modes: $\hat{H}_D = \hbar\omega_0 \sum_{\mu=1}^{N-1} \hat{D}_\mu^\dagger \hat{D}_\mu$. Eq. (5) can be further diagonalized, which leads to the following Hamiltonian:

$$\hat{H} = \hbar\omega_+ \hat{P}_+^\dagger \hat{P}_+ + \hbar\omega_- \hat{P}_-^\dagger \hat{P}_- + \hat{H}_D. \quad (6)$$

Here, the frequencies of the eigenstates are

$$\omega_\pm = \frac{1}{2} \left[\omega_0 + \omega_c \pm \sqrt{\Omega_N^2 + (\omega_0 - \omega_c)^2} \right]. \quad (7)$$

When the cavity photon and the bright mode are at resonance ($\omega_c = \omega_0$), the frequency difference between the two eigenstates is $\omega_+ - \omega_- = \Omega_N$. Once Ω_N exceeds the linewidth of the bright mode (which can be measured from the linear spectrum of molecules outside the cavity) and the loss rate of the cavity (due to the imperfections in the cavity mirrors), a peak splitting can be measured from the linear spectrum of the coupled cavity-molecular system. The peak splitting, which is called the collective Rabi splitting, is equal to $\Omega_N = 2\sqrt{N}g_0$.

In Eq. (6), the creation and annihilation operators for the eigenstates (\hat{P}_\pm^\dagger and \hat{P}_\pm) are defined as linear combinations of the cavity-photon and bright-mode operators:

$$\begin{aligned} \hat{P}_\pm &= X_\pm^{(B)} \hat{B} + X_\pm^{(c)} \hat{a}, \\ \hat{P}_\pm^\dagger &= X_\pm^{(B)} \hat{B}^\dagger + X_\pm^{(c)} \hat{a}^\dagger, \end{aligned} \quad (8)$$

where the coefficients are $X_+^{(B)} = -X_-^{(c)} = -\sin(\theta)$, $X_-^{(B)} = X_+^{(c)} = \cos(\theta)$, and the mixing angle θ is $\theta = \frac{1}{2} \tan^{-1} \left(\frac{\Omega_N}{\omega_c - \omega_0} \right)$. When a Rabi splitting is observed, the two eigenstates ($-$ and $+$) are called the lower (LP) or upper (UP) polariton, respectively.

1. Calculating polariton lifetime

In the absence of intermolecular interactions, as shown in Eq. (6), the polaritons are completely decoupled from the dark modes, so once the LP or UP is excited to the first excited state, the polaritonic decay rate ($1/\tau_\pm$) should be simply a linear combination of the relaxation rates of the photonic and the molecular parts^{63,64}:

$$\frac{1}{\tau_\pm} = |X_\pm^{(c)}|^2 k_c + |X_\pm^{(B)}|^2 k_B, \quad (9)$$

where k_c denotes the cavity loss rate, and k_B denotes the relaxation rate of the bright state from the first excited to the ground state outside a cavity, which could be approximated as the linewidth of the vibrational peak from molecular linear IR spectroscopy outside the cavity (if the molecular system has no inhomogeneous broadening). Note that the bright mode relaxation rate k_B reflects both the radiative and non-radiative relaxation pathways, and the radiative relaxation contribution can be superradiant (meaning a N dependence). For molecular vibrations, since the radiative relaxation rates (with a typical lifetime of seconds) are usually much slower than the non-radiative rates (with a typical lifetime from ns to ps), we will disregard the radiative relaxation contribution of k_B .⁶⁵

The rate equation in Eq. (9) has been widely known by the polariton community. For realistic molecular systems in the condensed phase, however, we need to consider another decay pathway of the polaritons. Since molecules do interact with each other, polaritons (which are partially composed the molecular degrees of freedom) can interact with the dark modes through intermolecular interactions. Naturally, the interaction between polaritons and dark modes may introduce an additional dephasing pathway for the decay of polaritons.

In order to account for this additional dephasing process, on top of the standard polaritonic Hamiltonian in Eq. (6), we add a simple tight-binding intermolecular interaction between neighboring molecules:

$$\hat{V} = \sum_{n=1}^N \hbar\Delta_n \left[\sum_{M_n=1}^{N_{nn}} \left(\hat{b}_n^\dagger \hat{b}_{M_n} + \hat{b}_n \hat{b}_{M_n}^\dagger \right) \right], \quad (10)$$

where M_n indices all the possible nearest neighbors (with a total number of N_{nn}) of molecule n , and Δ_n denotes the coupling strength between the nearest neighboring molecules. For different n , $\{\Delta_n\}$ are uncorrelated but should have similar magnitude. In Eq. (10), since the operators of each molecule can be expressed as linear combinations of the bright and dark modes, the interaction between bright (which contributes to the polaritons) and dark modes has been included. In order to better illustrate this point, if we consider only the bright-mode contribution of \hat{b}_{M_n} , i.e., $\hat{b}_{M_n} \leftarrow \hat{B}/\sqrt{N} + \dots$, we can approximate Eq. (10) as

$$\hat{V} = \frac{\hbar N_{nn}}{\sqrt{N}} \sum_{n=1}^N \Delta_n \left(\hat{b}_n^\dagger \hat{B} + \hat{b}_n \hat{B}^\dagger \right) + \dots, \quad (11)$$

where \dots represents the interaction between individual molecules (indexed by n) and the dark modes. For large N , since \hat{b}_n (\hat{b}_n^\dagger) is predominately composed of the dark modes, Eq. (11) can be used to calculate the polaritonic dephasing rate to the dark modes.

We now calculate the dephasing rate from polaritons to vibrational dark modes with a FGR calculation:

$$\gamma = \sum_f \frac{2\pi}{\hbar^2} |V_{fi}|^2 \delta(\omega - \omega_f). \quad (12a)$$

Here i and f denotes the initial (polaritonic) and final (dark) states; $\delta(\omega - \omega_f)$ denotes the density of states (DOS) for state f ; $V_{fi} = \langle f | \hat{V} | i \rangle$ denotes the transition matrix element, where we have defined \hat{V} in (11). By substituting $|i\rangle = \hat{P}_\pm^\dagger |0\rangle$ (exciting a polariton) and the definition of \hat{P}_\pm^\dagger in Eq. (8), and by also approximating $|f\rangle \approx \hat{b}_f^\dagger |0\rangle$ (exciting an individual molecular vibration, which is mostly composed of the dark modes under a large N), we obtain the transition matrix element as:

$$V_{fi} = \langle f | \hat{V} | i \rangle \approx \frac{\hbar N_{nn} \Delta_f}{\sqrt{N}} X_\pm^{(B)}. \quad (13)$$

Hence, the polaritonic dephasing rate becomes

$$\begin{aligned} \gamma_\pm &\approx \sum_{f=1}^N \frac{2\pi}{\hbar^2} \left(\frac{\hbar N_{nn} \Delta_f}{\sqrt{N}} X_\pm^{(B)} \right)^2 \delta(\omega - \omega_f), \\ &= 2\pi \Delta^2 |X_\pm^{(B)}|^2 \rho_0(\omega), \end{aligned} \quad (14)$$

Here, we have defined $\Delta^2 \equiv \sum_{f=1}^N N_{nn}^2 \Delta_f^2 \delta(\omega - \omega_f) / \sum_{f=1}^N \delta(\omega - \omega_f)$ to denote the average intermolecular coupling strength; $\rho_0(\omega) \equiv \frac{1}{N} \sum_{f=1}^N \delta(\omega - \omega_f)$ denotes the DOS for the dark-mode manifold per molecule. Note that here we have assumed that polariton states are orthogonal to the individual molecular basis ($\{\hat{b}_n\}$), which is valid in the limit of large N .

In reality, since the polaritonic state has also a linewidth, we may introduce a normalized DOS for the polariton ($\rho_\pm(\omega)$, where $\int_{-\infty}^{\infty} d\omega \rho_\pm(\omega) = 1$) to smear out the dephasing rate:

$$\gamma_\pm = 2\pi \Delta^2 |X_\pm^{(B)}|^2 J_\pm, \quad (15a)$$

where J_\pm denotes the spectral overlap between the polariton and the dark modes:

$$J_\pm \equiv \int_0^{+\infty} d\omega \rho_0(\omega) \rho_\pm(\omega). \quad (15b)$$

Eq. (15) shows that the polaritonic dephasing rate is determined by three factors: the magnitude of intermolecular interactions (Δ^2), the molecular weight of polaritons ($|X_\pm^{(B)}|^2$), and the spectral overlap between the polariton and dark modes (J_\pm). This equation is reminiscent of the Förster resonance energy transfer rate⁶⁶. Note that the linear relationship between the polariton dephasing rate and the spectral overlap has been numerically demonstrated for exciton-polaritons⁴⁹. Similar analytic results as Eq. (15) have also been obtained previously^{42,46}.

Finally, given Eq. (9) and Eq. (15), the observed polariton lifetime becomes

$$\frac{1}{\tau_\pm} = |X_\pm^{(c)}|^2 k_c + |X_\pm^{(B)}|^2 k_B + \gamma_\pm(k_c, k_B). \quad (16)$$

Here, we write $\gamma_\pm(k_c, k_B)$ (instead of γ_\pm) to emphasize the fact that the polaritonic dephasing rate γ_\pm does depend on k_c and k_B , whose values can modify J_\pm by altering the polaritonic lineshape (see Eq. (15b)).⁶⁷ In this sense, the difference between Eq. (16) and Eq. (9) not only comes from the introduction of the polaritonic dephasing rate γ_\pm (which arises from intermolecular interactions), but also stems from the more complicated parameter dependence on k_c and k_B , e.g., $\partial(1/\tau_\pm)/\partial k_c = |X_\pm^{(c)}|^2 + \partial\gamma_\pm/\partial k_c \neq |X_\pm^{(c)}|^2$. See Appendix S-II for a detailed discussion.

For Eq. (16), let us consider the limit when the cavity and the bright modes are decoupled. In this limit, Eq. (16) is expected to recover the lifetimes of the cavity and the bright mode, respectively. For example, in the limit of a highly red-detuned cavity mode ($\omega_c \ll \omega_0$), the "LP" is mostly composed of the cavity mode ($|X_-^{(c)}|^2 \rightarrow 1$ and $|X_-^{(B)}|^2 \rightarrow 0$) and the "UP" is mostly composed of the bright mode ($|X_+^{(c)}|^2 \rightarrow 0$ and $|X_-^{(B)}|^2 \rightarrow 1$). The lifetimes of the two "polaritons" become

$$\frac{1}{\tau_-} \rightarrow k_c, \quad (17a)$$

$$\frac{1}{\tau_+} \rightarrow k_B + 2\pi \Delta^2 \int_0^{+\infty} d\omega \rho_0(\omega) \rho_0(\omega). \quad (17b)$$

At this limit, the "LP" lifetime is the inverse of the cavity loss rate (k_c), and the "UP" lifetime becomes the inverse of the bright-mode relaxation (k_B) plus the dephasing rates ($2\pi \Delta^2 \int_0^{+\infty} d\omega \rho_0(\omega) \rho_0(\omega)$) outside a cavity. This expected result shows the self-consistency of Eq. (16).

B. CavMD simulations of polariton lifetime

Apart from the above analytic approach, the recently developed CavMD simulations^{45,52} can also be used to

determine the polariton lifetime under VSC. Within the framework of CavMD, the coupled photon-nuclear dynamics are propagated on an electronic ground-state surface. The light-matter Hamiltonian for CavMD is defined as follows:

$$\hat{H}_{\text{QED}}^{\text{G}} = \hat{H}_{\text{M}}^{\text{G}} + \hat{H}_{\text{F}}^{\text{G}}, \quad (18a)$$

where $\hat{H}_{\text{M}}^{\text{G}}$ is the conventional molecular (kinetic + potential) Hamiltonian on an electronic ground-state surface outside a cavity, and $\hat{H}_{\text{F}}^{\text{G}}$ denotes the field-related Hamiltonian:

$$\begin{aligned} \hat{H}_{\text{F}}^{\text{G}} = & \sum_{k,\lambda} \frac{\hat{p}_{k,\lambda}^2}{2m_{k,\lambda}} \\ & + \frac{1}{2} m_{k,\lambda} \omega_{k,\lambda}^2 \left(\hat{q}_{k,\lambda} + \frac{\varepsilon_{k,\lambda}}{m_{k,\lambda} \omega_{k,\lambda}^2} \sum_{n=1}^N \hat{d}_{ng,\lambda} \right)^2. \end{aligned} \quad (18b)$$

Here, $\hat{p}_{k,\lambda}$, $\hat{q}_{k,\lambda}$, $\omega_{k,\lambda}$, and $m_{k,\lambda}$ denote the momentum operator, position operator, frequency, and the auxiliary mass for the cavity photon mode defined by a wave vector \mathbf{k} and polarization direction $\boldsymbol{\xi}_{\lambda}$. The auxiliary mass $m_{k,\lambda}$ introduced here is solely for the convenience of molecular dynamics simulations, and the value of $m_{k,\lambda}$ does not change the VSC dynamics.^{45,52} $\hat{d}_{ng,\lambda}$ denotes the electronic ground-state dipole operator for molecule n projected along the direction of $\boldsymbol{\xi}_{\lambda}$. $\varepsilon_{k,\lambda} \equiv \sqrt{m_{k,\lambda} \omega_{k,\lambda}^2 / \Omega \epsilon_0}$ characterizes the coupling strength between each cavity photon and individual molecule, where Ω denotes the cavity mode volume and ϵ_0 denotes the vacuum permittivity.

In order to reduce the computational cost, we (i) map all quantum operators in Eq. (18) to classical variables and also (ii) apply periodic boundary conditions for the molecular degrees of freedom, i.e., in Eq. (18b) we assume $\sum_{n=1}^N d_{ng,\lambda} = N_{\text{cell}} \sum_{n=1}^{N_{\text{sub}}} d_{ng,\lambda}$, where N_{cell} denotes the number of the periodic cells and $N_{\text{sub}} = N/N_{\text{cell}}$ is the number of molecules in a single simulation cell. By also denoting $\tilde{q}_{k,\lambda} = \tilde{q}_{k,\lambda} / \sqrt{N_{\text{cell}}}$ and an effective light-matter coupling strength

$$\tilde{\varepsilon}_{k,\lambda} \equiv \sqrt{N_{\text{cell}}} \varepsilon_{k,\lambda} = \sqrt{\frac{N_{\text{cell}} m_{k,\lambda} \omega_{k,\lambda}^2}{\Omega \epsilon_0}}, \quad (19)$$

we obtain classical equations of motion for the coupled photon-nuclear system that are suitable for practical simulations:

$$M_{nj} \ddot{\mathbf{R}}_{nj} = \mathbf{F}_{nj}^{(0)} + \mathbf{F}_{nj}^{\text{cav}} + \mathbf{F}_{nj}^{\text{ext}}(t) \quad (20a)$$

$$m_{k,\lambda} \ddot{\tilde{q}}_{k,\lambda} = -m_{k,\lambda} \omega_{k,\lambda}^2 \tilde{q}_{k,\lambda} - \tilde{\varepsilon}_{k,\lambda} \sum_{n=1}^{N_{\text{sub}}} d_{ng,\lambda} \quad (20b)$$

Here, the subscript nj denotes the j -th atom in molecule n ; $\mathbf{F}_{nj}^{(0)}$ denotes the force on each nucleus outside a cavity;

$$\mathbf{F}_{nj}^{\text{cav}} = - \sum_{k,\lambda} \left(\tilde{\varepsilon}_{k,\lambda} \tilde{q}_{k,\lambda} + \frac{\tilde{\varepsilon}_{k,\lambda}^2}{m_{k,\lambda} \omega_{k,\lambda}^2} \sum_{l=1}^{N_{\text{sub}}} d_{lg,\lambda} \right) \frac{\partial d_{ng,\lambda}}{\partial \mathbf{R}_{nj}}$$

denotes the cavity force on each nucleus; $\mathbf{F}_{nj}^{\text{ext}}(t) = Q_{nj} \mathbf{E}_{\text{ext}}(t)$ denotes an external force on each nucleus [with partial charge Q_{nj} (due to the bare nuclear charge plus the shielding effect due to the surrounding electrons)] due to a time-dependent electric field ($\mathbf{E}_{\text{ext}}(t)$). Note that, since our goal is to excite the polariton (which is a hybrid light-matter state), it is equivalent to either pump the cavity mode or pump the molecules given the fast energy exchange between these two subsystems (which is characterized by the Rabi splitting). In Eq. (20), we have chosen to excite the molecular subsystem just for simplicity [to avoid the introduction of a new phenomenological term when pumping the cavity mode is considered (namely the effective transition dipole moment of the cavity mode)].

1. Calculating polariton lifetime

The numerical scheme in Eq. (20) allows us to calculate of the polariton lifetime by performing a nonequilibrium CavMD simulation after an IR pulse excitation. Following the method and simulation details in Ref.⁴⁵, we capture the polariton lifetime as follows. We consider a liquid CO₂ system (where $N_{\text{sub}} = 216$) in a cubic simulation cell with a cell length of 24.292 Å (which corresponds to a molecular density of 1.101 g/cm³). This molecular system is coupled to a cavity mode with two polarization directions (along x and y); see the cartoon in Fig. 1 for the simulation setup. At $t = 0$, the coupled cavity-molecular system has been thermally equilibrated under an NVT (constant molecular number, volume, and temperature) ensemble with an Langevin thermostat applied to all particles (nuclei + photons). If we assume no cavity loss, when $t > 0$, the equilibrated system is propagated under an NVE (constant molecular number, volume, and energy) ensemble, and the polariton is pumped by sending an external x -polarized pulse

$$\mathbf{E}_{\text{ext}}(t) = E_0 \cos(\omega t + \phi) \mathbf{e}_x \quad (21)$$

during a time interval $t_{\text{start}} < t < t_{\text{end}}$ ps, where the pulse frequency $\omega = \omega_{\pm}$ excites either the LP or UP and ϕ denotes a random phase. For parameters, we set $t_{\text{start}} = 0.1$ ps, $t_{\text{end}} = 0.6$ ps, $E_0 = 3.084 \times 10^6$ V/m (6×10^{-4} a.u.), so the input pulse fluence is $F = \frac{1}{2} \epsilon_0 c E_0^2 (t_{\text{end}} - t_{\text{start}}) = 6.32$ mJ/cm². On the one hand, such a pulse fluence is weak enough to minimize the possible nonlinear absorption channel due to molecular anharmonicity, so it is possible to compare CavMD results with the FGR rate derived from a harmonic model; on the other hand, the pulse fluence is also strong enough so that the polariton relaxation signal overcomes thermal and computational noise. See Fig. 6 in Appendix S-I for the profile of this pulse in both the time and frequency domains.

Immediately after the polariton pumping, we monitor the time-resolved dynamics of the cavity photon energy $E_{\text{ph}} = \sum_{\lambda=x,y} \tilde{p}_{\lambda}^2 / 2m_c + \frac{1}{2} m_c \omega_c^2 \tilde{q}_{\lambda}^2$, where we have set the auxiliary photonic mass $m_c = 1$ a.u. for simplicity. By fitting the cavity photon energy dynamics (which is

averaged by 40 trajectories) with an exponential function, we obtain the polariton lifetime. See Ref.⁴⁵ for all necessary simulation details. Note that during the above NVE simulation, although the cavity loss has been ignored, bright-mode relaxation and dephasing processes have been included explicitly due to an explicit propagation of all molecular degrees of freedom.

In order to further include the effect of cavity loss, during the nonequilibrium simulation, we attach a Langevin thermostat to the cavity mode only⁵³. Here, the friction lifetime of the Langevin thermostat defines the inverse of the cavity loss rate. The procedure for obtaining the polariton lifetime remains the same as above.

C. Connecting the FGR rate to CavMD simulations

We have introduced two (analytic + numerical) approaches to obtain the polariton lifetime. Both approaches have advantages and disadvantages. On the one hand, while the FGR rate in Eqs. (15) and (16) is very straightforward, this rate relies on many parameters, including the cavity loss rate, bright-mode relaxation rate, the Rabi splitting and cavity mode detuning (to determine X_{\pm}^B and X_{\pm}^c), the DOS of dark modes and the polaritons and intermolecular coupling Δ (to determine the dephasing rate). In short, the FGR rate relies heavily on the experimental input.

On the other hand, despite the practical simplicity of CavMD, the polariton lifetime obtained from nonequilibrium CavMD relies heavily on the accuracy of molecular force fields. While state-of-art molecular dynamics techniques allow an accurate description of both molecular DOS and the relaxation rate^{68–71}, an experimentally accurate simulation can be very nontrivial.

With this background in mind, we will compare CavMD and the FGR rate as follows. With the anharmonic CO₂ force field⁴⁵ (which largely resembles the CO₂ force field in Ref.⁷² except for the use of an anharmonic C=O bond potential), we will directly obtain the polariton decay rate from nonequilibrium CavMD simulations after sending a pulse to excite the polariton; we will also obtain the polariton and molecular DOS from equilibrium CavMD simulations. Thereafter, we will calculate the FGR rate and check for internal consistency.

Let us now introduce how to estimate the FGR rate from equilibrium CavMD results in practice.

1. Practical way to calculate $|X_{\pm}^{(B)}|^2 J_{\pm}$ from equilibrium CavMD simulations

For the FGR rate, among all parameters in Eqs. (15) and (16), the most nontrivial property related to the strong coupling is the molecule-weighted spectral overlap integral ($|X_{\pm}^{(B)}|^2 J_{\pm}$ in Eq. (15)). Here, we will demonstrate how to calculate this property practically.

Since the equilibrium IR absorption spectrum can be easily obtained from both experiments and equi-

librium CavMD simulations, in the expression for J_{\pm} , we approximate the DOS of the dark modes $[\rho_0(\omega)]$ as the normalized molecular linear IR absorption lineshape outside the cavity, or $\rho_{\text{IR, outcav}}(\omega)/\mathcal{N}_0$, where $\mathcal{N}_0 = \int_{\omega_{\min}}^{\omega_{\max}} d\omega \rho_{\text{IR, outcav}}(\omega)$ denotes the normalization factor and ω_{\min} and ω_{\max} denote the lower and upper limits of the vibrational lineshape. Similarly, we approximate the DOS of the LP or UP $[\rho_{\pm}(\omega)]$ as the normalized linear molecular IR absorption lineshape for the polariton, respectively. Note that, because the LP and UP lineshapes appear together in the molecular IR spectrum inside the cavity $[\rho_{\text{IR, incav}}(\omega)]$, here we simply assign a dividing frequency $\omega_{\text{mid}} \equiv (\omega_- + \omega_+)/2$ to separate the LP and UP and obtain the lineshapes for them, respectively. Quantitatively, we can calculate $|X_{\pm}^{(B)}|^2 J_{\pm}$ as follows:

$$|X_-^{(B)}|^2 J_- \approx \frac{|X_-^{(B)}|^2}{\mathcal{N}_0 \mathcal{N}_{\text{LP}}} \int_{\omega_{\min}}^{\omega_{\text{mid}}} d\omega \rho_{\text{IR, outcav}}(\omega) \rho_{\text{IR, incav}}(\omega), \quad (22a)$$

$$|X_+^{(B)}|^2 J_+ \approx \frac{|X_+^{(B)}|^2}{\mathcal{N}_0 \mathcal{N}_{\text{UP}}} \int_{\omega_{\text{mid}}}^{\omega_{\max}} d\omega \rho_{\text{IR, outcav}}(\omega) \rho_{\text{IR, incav}}(\omega). \quad (22b)$$

The integral in Eq. (22a) spans from ω_{\min} to ω_{mid} , which accounts for the spectral overlap between the LP and the dark modes; similarly, the integral in Eq. (22b) spans from ω_{mid} to ω_{\max} , which accounts for the spectral overlap between the UP and the dark modes. The denominators above ensure the normalization of the corresponding lineshapes:

$$\mathcal{N}_0 = \int_{\omega_{\min}}^{\omega_{\max}} d\omega \rho_{\text{IR, outcav}}(\omega), \quad (22c)$$

$$\mathcal{N}_{\text{LP}} = \int_{\omega_{\min}}^{\omega_{\text{mid}}} d\omega \rho_{\text{IR, incav}}(\omega), \quad (22d)$$

$$\mathcal{N}_{\text{UP}} = \int_{\omega_{\text{mid}}}^{\omega_{\max}} d\omega \rho_{\text{IR, incav}}(\omega). \quad (22e)$$

Note that, from our previous study⁵², we have learned that the integrated peak area of the LP (or UP) is proportional to the molecular weight ($|X_{\pm}^{(B)}|^2$) times a correction factor (which transforms a classical dipole autocorrelation function to an experimentally comparable IR spectrum), i.e., $\int_{\omega_{\min}}^{\omega_{\text{mid}}} d\omega \rho_{\text{IR, incav}}(\omega) / \int_{\omega_{\min}}^{\omega_{\max}} d\omega \rho_{\text{IR, incav}}(\omega) \sim |X_-^{(B)}|^2$ and $\int_{\omega_{\text{mid}}}^{\omega_{\max}} d\omega \rho_{\text{IR, incav}}(\omega) / \int_{\omega_{\min}}^{\omega_{\max}} d\omega \rho_{\text{IR, incav}}(\omega) \sim |X_+^{(B)}|^2$ (where we have assumed that the correction factor can be largely eliminated between the numerator and denominator). Hence, we may rewrite Eq. (22) in a simpler form:

$$|X_-^{(B)}|^2 J_- \approx \frac{1}{\mathcal{N}} \int_{\omega_{\min}}^{\omega_{\text{mid}}} d\omega \rho_{\text{IR, outcav}}(\omega) \rho_{\text{IR, incav}}(\omega), \quad (23a)$$

$$|X_+^{(B)}|^2 J_+ \approx \frac{1}{\mathcal{N}} \int_{\omega_{\text{mid}}}^{\omega_{\max}} d\omega \rho_{\text{IR, outcav}}(\omega) \rho_{\text{IR, incav}}(\omega), \quad (23b)$$

where

$$\mathcal{N} = \int_{\omega_{\min}}^{\omega_{\max}} d\omega \rho_{\text{IR, incav}}(\omega) \int_{\omega_{\min}}^{\omega_{\max}} d\omega' \rho_{\text{IR, outcav}}(\omega'). \quad (23c)$$

This expression avoids directly evaluating $|X_{\pm}^{(B)}|^2$ and appears easier to handle compared with Eq. (22). Note that it is preferable to avoid evaluating $|X_{\pm}^{(B)}|^2$ explicitly since, in CavMD, the inclusion of the self-dipole term in the Hamiltonian (18) leads to a slightly different expression for $|X_{\pm}^{(B)}|^2$ relative to the quantum model (where the self-dipole term is excluded — although when the Rabi splitting is small, such difference is always negligible⁵²).

By comparing the polariton lifetime fitted from nonequilibrium CavMD simulations and $|X_{\pm}^{(B)}|^2 J_{\pm}$ in Eq. (23), we can evaluate the inherent consistency and validity of CavMD as far as describing the polariton relaxation process.

D. Evaluating IR spectroscopy

For the sake of completeness, the equation we use to numerically evaluate the molecular IR spectrum outside the cavity is given as follows^{73–76}:

$$n(\omega)\alpha(\omega) = \frac{\pi\beta\omega^2}{2\epsilon_0 V c} \frac{1}{2\pi} \int_{-\infty}^{+\infty} dt e^{-i\omega t} \langle \boldsymbol{\mu}_S(0) \cdot \boldsymbol{\mu}_S(t) \rangle. \quad (24)$$

Here, $\alpha(\omega)$ denotes the absorption coefficient, $n(\omega)$ denotes the refractive index, V is the volume of the system (i.e., the simulation cell), c denotes the speed of light, $\beta = k_B T$, and $\boldsymbol{\mu}_S(t)$ denotes the *total* dipole moment of the molecules at time t . Similarly, inside the cavity, we evaluate the IR spectrum as follows:

$$n(\omega)\alpha(\omega) = \frac{\pi\beta\omega^2}{2\epsilon_0 V c} \frac{1}{2\pi} \int_{-\infty}^{+\infty} dt e^{-i\omega t} \times \left\langle \sum_{i=x,y} (\boldsymbol{\mu}_S(0) \cdot \mathbf{e}_i) (\boldsymbol{\mu}_S(t) \cdot \mathbf{e}_i) \right\rangle, \quad (25)$$

where \mathbf{e}_i denotes the unit vector along direction $i = x, y$. Different from Eq. (25), inside the cavity, since the supposedly z -oriented cavity (see the cartoon in Fig. 1) is coupled to the molecular dipole moment along the x and y directions, only these two components of the molecular dipole moment are included when we calculate the IR spectrum of the polaritons.

III. RESULTS AND DISCUSSION

According to the analytic expression in Eq. (16), the polariton lifetime is determined by three factors: (i) the vibrational relaxation rate of the bright mode (to the ground state) outside the cavity k_B , (ii) the cavity loss rate k_c , and (iii) the polariton dephasing rate to the dark modes γ_{\pm} . As far as k_B is considered, since the bright

and the dark modes are degenerate outside the cavity, the vibrational relaxation rates of the bright and dark modes should also be the same, equal to the vibrational relaxation rates of individual molecules. For the liquid CO_2 system we simulate, since the vibrational relaxation rate outside the cavity is the smallest ($\sim 0.03 \text{ ps}^{-1}$),⁵³ while the other two factors usually take a rate of $\sim \text{ps}^{-1}$, below we will neglect the contribution of k_B to the polariton lifetime and focus only on the contributions of k_c and γ_{\pm} .

A. Role of cavity loss

1. Liquid CO_2

Let us first investigate the polariton lifetime dependence on the cavity loss rate k_c when a liquid CO_2 system (with a molecular density of 1.101 g/cm^3) forms VSC. The Fig. 2a inset plots the equilibrium IR spectrum outside a cavity (black line; see Eq. (24) for the definition). Here, the C=O asymmetric stretch of CO_2 peaks at 2327 cm^{-1} , in good agreement with experimental values⁷⁷. When a cavity mode (with two polarization directions) at 2320 cm^{-1} (denoted as the vertical blue line in the inset of Fig. 2a) is coupled to the molecular subsystem with an effective coupling strength $\tilde{\epsilon} = 2 \times 10^{-4}$ a.u., a pair of UP (peaked at $\omega_+ = 2428 \text{ cm}^{-1}$) and LP (peaked at $\omega_- = 2241 \text{ cm}^{-1}$) is observed in the molecular IR spectrum (red line; see Eq. (25) for the definition).

Under VSC conditions, Fig. 2a plots the photonic energy dynamics when the UP is resonantly pumped by a relatively weak external E-field $[\mathbf{E}_{\text{ext}}(t) = E_0 \cos(\omega t + \phi)\mathbf{e}_x]$ with fluence 6.32 mJ/cm^2 and a 0.5 ps duration, which is labeled as a yellow shadow; see Sec. IIB 1 for details on the IR excitation. When the cavity lifetime ($\tau_c = 1/k_c$) is tuned from ∞ (orange line) to 0.3 ps (black line), the photonic energy decays faster. In Fig. 2a, the fast oscillations (with a period of $\sim 0.2 \text{ ps}$) during the photonic energy decay is in agreement with the Rabi splitting ($187 \text{ cm}^{-1} = 0.18 \text{ ps}^{-1}$), indicating a fast coherent energy exchange between cavity photons and the C=O asymmetric stretch. Note that for Fabry–Pérot VSC, the experimental cavity lifetime usually takes $1 \sim 10 \text{ ps}$ ²⁷.

Since cavity photons contribute to the polaritons, we can extract the polariton lifetime ($1/\tau_{\pm}$) by fitting the photonic energy dynamics with an exponential function after the IR excitation (when $t > 0.6 \text{ ps}$). Fig. 2c plots the fitted UP lifetime ($1/\tau_+$) versus the cavity loss rate (magenta circles). A linear fit of the UP lifetime data yields a slope of 0.58 , meaning that roughly half of the cavity loss rate contributes to the polariton decay.

After investigating the UP lifetime, we study the LP lifetime dependence on the cavity loss rate. Similarly, Fig. 2b plots the photonic energy dynamics when the LP is resonantly excited by the external E-field with the same fluence (6.32 mJ/cm^2) as the UP excitation. Fig. 2c plots the fitted LP decay rate versus the cavity loss

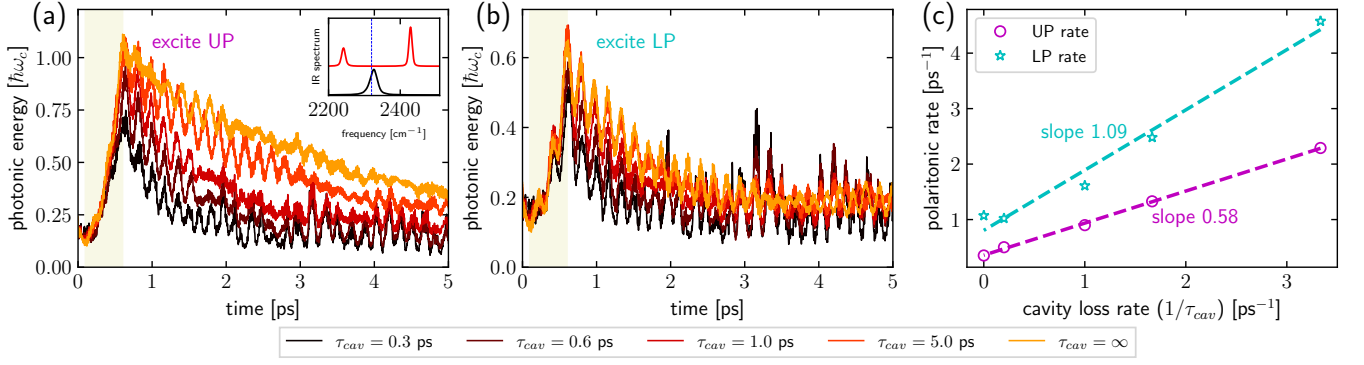


FIG. 2. The polariton lifetime for liquid CO₂ under VSC as a function of cavity loss ($k_c = 1/\tau_c$). Time-resolved cavity photon energy dynamics after a weak (a) UP or (b) LP excitation. Lines with different colors denote different cavity lifetimes (from black to yellow, the cavity lifetime spans from $\tau_c = 1/k_c = 0.3$ ps to $+\infty$; see the legend). The inset of Fig. a plots the equilibrium IR spectrum of liquid CO₂ outside (black) or inside (red) the cavity, where the cavity mode frequency is 2200 cm⁻¹ (the vertical blue dashed line) and the effective coupling strength is $\tilde{\epsilon} = 2 \times 10^{-4}$ a.u. (c) The corresponding fitted polaritonic decay rate ($1/\tau_{\pm}$) versus the cavity loss rate ($k_c = 1/\tau_c$) for the UP (magenta circles) and the LP (cyan stars). The slopes of the linear fits (dashed lines) are labeled accordingly. See Sec. II B 1 for other simulation details.

rate (cyan stars), where the slope of the LP data is 1.09.

At this moment, we cannot make an immediate connection between the CavMD results with the analytic rate in Eq. (16). As emphasized below Eq. (16) (see also Appendix S-II), since changing the value of k_c not only directly modifies $|X_{\pm}^{(c)}|^2$, but also indirectly alters the polaritonic dephasing rate γ_{\pm} through the polaritonic lineshape, the slope obtained by fitting $1/\tau_{\pm}$ versus k_c (as in Fig. 2c) does not necessarily recover $|X_{\pm}^{(c)}|^2$ —it is $|X_{\pm}^{(c)}|^2 + \partial\gamma_{\pm}/\partial k_c$ instead. Therefore, only when γ_{\pm} is not very sensitive to k_c ($|\partial\gamma_{\pm}/\partial k_c| \ll |X_{\pm}^{(c)}|^2$), we expect to obtain the agreement between the fitted slope and $|X_{\pm}^{(c)}|^2$. In our case, the cavity mode and the C=O asymmetric stretch are near resonance, so the cavity weight of the polariton ($|X_{\pm}^{(c)}|^2$) is roughly a half. In Fig. 2c, we have observed that the fitted slope for the UP (not the LP) agrees well with $|X_{+}^{(c)}|^2$. Because the value of $\partial\gamma_{\pm}/\partial k_c$ is unknown, however, the agreement between the UP fitted slope and $|X_{+}^{(c)}|^2$ cannot fully verify any consistency between CavMD and the analytic rate, not to mention the LP data.

2. A Diluted CO₂ ensemble

In order to better compare the CavMD results with the analytic expression in Eq. (16), we need to exclude the influence of polaritonic dephasing in the CavMD results (note that k_B is always negligibly small for our simulations). This can be achieved, since $\gamma_{\pm} \propto \Delta^2$ (Eq. (15)), by reducing intermolecular interactions (Δ) or equivalently decreasing the CO₂ molecular density. Hence, we further repeat our simulation in Fig. 2 with a diluted CO₂ ensemble (with a density of 0.073 g/cm³). The molecular density is reduced by increasing the simulation cell length to 60.0 Å while fixing N_{sub} , the molecular

number in the cell, so the Rabi splitting remains the same (see the inset of Fig. 3a). By controlling all the other simulation details the same as Fig. 2, in Fig. 3 we replot the photonic energy dynamics for the (a) UP and (b) LP as well as (c) the fitted polaritonic decay rates versus the cavity loss rate. As shown in Fig. 3c, the fitted slopes for both the UP and LP are nearly a half, in agreement with $|X_{\pm}^{(c)}|^2$. Because here we have greatly suppressed the polaritonic dephasing rate by decreasing the molecular density, Fig. 3c confirms the consistency between CavMD and the analytic rate in Eq. (16) when the cavity loss dependence is considered.

As a short summary of this part, we have observed that, if the polaritonic dephasing rate is negligible, both CavMD and the analytic expression (Eq. (16)) predict a similar dependence for the polaritonic decay rate as a function of the cavity loss, i.e., $|X_{\pm}^{(c)}|^2$ of the cavity loss rate enters the polaritonic decay rate. While the fitted slope of the UP is always $|X_{\pm}^{(c)}|^2$ times the cavity loss rate for both Figs. 2 and 3, the LP results for liquid CO₂ (see Fig. 2) no longer shows this dependence on the cavity loss. The deviation for the LP is an example for the complicated interplay between cavity loss and polaritonic dephasing under liquid-phase VSC, which might prevent the LP from forming a more coherent and long-lived state than the cavity photon mode.

B. Role of polariton dephasing to the dark modes

Next, let us focus on the effect of polariton dephasing on the polariton lifetime. For the results below, we set the cavity loss rate to be zero. Since the bright-mode relaxation rate k_B is much smaller than the dephasing rate, below the fitted polariton decay rate from CavMD simulations should largely equal to the polaritonic dephasing rate.

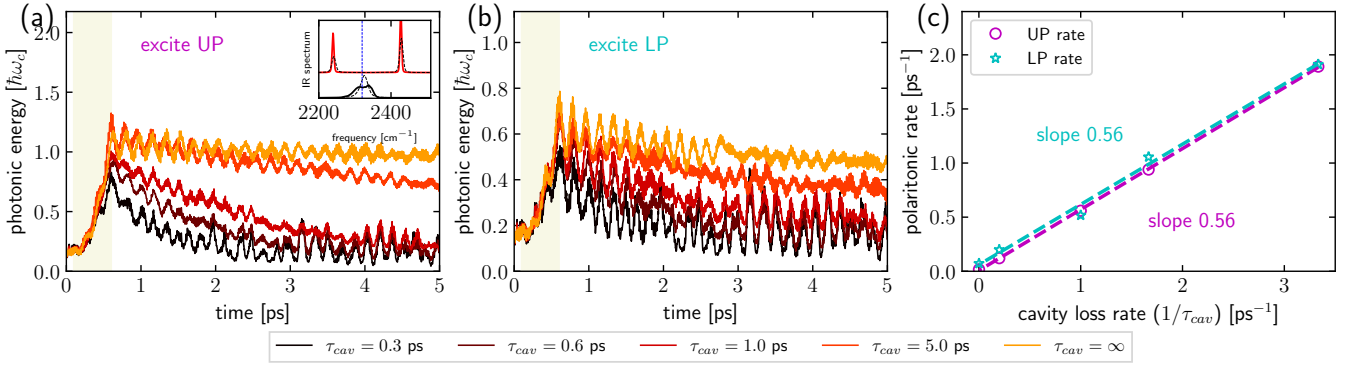


FIG. 3. The same plot as Fig. 2 when the CO₂ molecular density is decreased from 1.101 g/cm³ to 0.073 g/cm³ and all other simulation details are kept the same. In Fig. (a) inset the dashed thin black lines are the corresponding spectra in Fig. 2 and the solid lines are the spectra when the density is reduced. As shown in the inset, the Rabi splitting is largely unchanged when the molecular density changes.

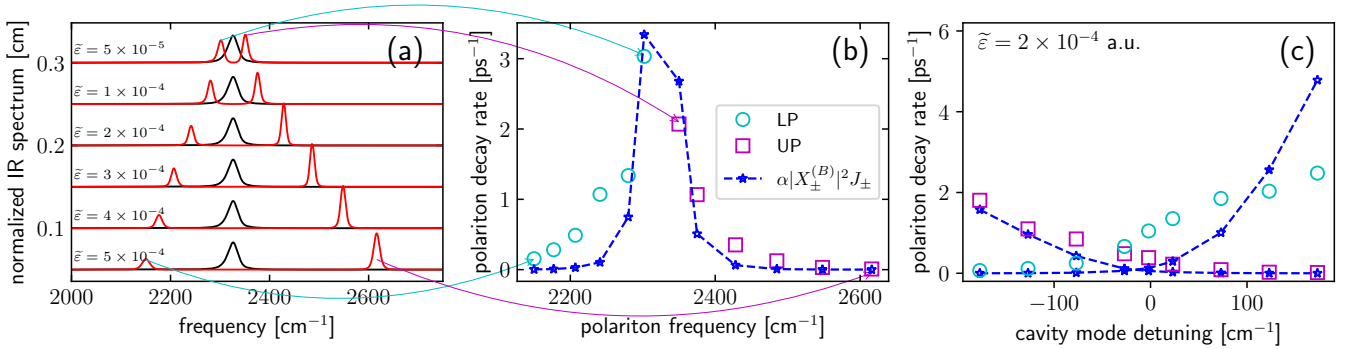


FIG. 4. Polariton decay rate versus Rabi splitting and cavity mode detuning. (a) Simulated IR spectrum for liquid CO₂ inside (red lines) or outside (black lines) a cavity. The cavity mode frequency (ω_c) is set as 2320 cm⁻¹. From bottom to top, the effective coupling strength is labeled on each lineshape (from 5×10^{-5} a.u. to 5×10^{-4} a.u.), respectively. (b) Simulated polariton decay rate for the polaritons in Fig. a (cyan circles for the LP and magenta squares for the UP; same as below). Blue stars plot $\alpha|X_{\pm}^{(B)}|^2 J_{\pm}$, where $|X_{\pm}^{(B)}|^2 J_{\pm}$ is defined in Eq. (23) and $\alpha = 1200$ ps⁻¹/cm is a prefactor to best fit the polaritonic decay rates. (c) Polariton decay rate and the corresponding $\alpha|X_{\pm}^{(B)}|^2 J_{\pm}$ versus the cavity mode detuning ($\omega_c - \omega_0$) when $\tilde{\epsilon} = 2 \times 10^{-4}$ a.u., where α takes the same value as that in Fig. b. See Sec. II B 1 for other simulation details.

1. Rabi splitting dependence

Fig. 4a plots the equilibrium IR spectrum calculated from CavMD simulations. Here, the cavity mode frequency is $\omega_c = 2320$ cm⁻¹, and the effective light-matter coupling strength is set from $\tilde{\epsilon} = 5 \times 10^{-5}$ a.u. to 5×10^{-4} a.u. (red lines from bottom to top; see the text on each lineshape which labels the corresponding $\tilde{\epsilon}$). We have also plotted the equilibrium IR spectrum outside the cavity (black lines) for comparison.

For every polariton shown in Fig. 4a, Fig. 4b plots the polariton dephasing rate from nonequilibrium CavMD simulations when a weak pulse (with fluence 6.32 mJ/cm²) resonantly excites the corresponding polariton. Here, the fitted LP (cyan circles) and UP (magenta squares) decay rates are plotted as a function of the polaritonic peak frequency (see Fig. 4a). As mentioned

above, because the bright-mode relaxation rate k_B is intrinsically small and we have also set the cavity loss rate to zero, the fitted polariton lifetime from nonequilibrium CavMD simulations should capture the polariton dephasing rate.

In order to explicitly compare the simulated polaritonic dephasing rate with the FGR calculation, Fig. 4b also plots the molecule-weighted spectral overlap ($|X_{\pm}^{(B)}|^2 J_{\pm}$; blue stars) for the polaritons by numerically evaluating Eq. (23) given the lineshapes in Fig. 4a. Here, in order to directly compare with the polariton dephasing rate from CavMD simulations, we multiply a prefactor $\alpha = 1200$ ps⁻¹/cm on top of $|X_{\pm}^{(B)}|^2 J_{\pm}$, where the prefactor α is chosen to best fit the CavMD dephasing rates. In Fig. 4b, the $\alpha|X_{\pm}^{(B)}|^2 J_{\pm}$ values and the fitted rates generally agree with each other (especially for the UP). Both the UP and LP results show a maxi-

imum when the polariton frequency is closer to the C=O asymmetric stretch outside the cavity ($\omega_0 = 2327 \text{ cm}^{-1}$). However, the agreement disappears for the LP regime near 2241 cm^{-1} , where the CavMD rates are larger than the $\alpha|X_{\pm}^{(B)}|^2 J_{\pm}$ values. Such a disagreement can be explained by the polariton-enhanced molecular nonlinear absorption mechanism⁴⁵: when the LP frequency is close to 2241 cm^{-1} , since twice the LP is near resonance with $0 \rightarrow 2$ vibrational transition of the dark modes, an additional nonlinear dephasing mechanism occurs for the LP and causes a faster LP dephasing rate than that from a harmonic model ($|X_{\pm}^{(B)}|^2 J_{\pm}$). Because the pulse fluence we use here is not very strong, the nonlinear effect does not dominate the polariton dephasing, and only a modest disagreement between the fitted rates and $|X_{\pm}^{(B)}|^2 J_{\pm}$ appears for the LP regime.

2. Detuning dependence

After studying how vibrational relaxation and polaritonic dephasing depends on the Rabi splitting, we will now address how these observables depend on the cavity mode frequency detuning. When we set the effective coupling strength to $\tilde{\varepsilon} = 2 \times 10^{-4} \text{ a.u.}$ and tune the cavity mode frequency from 2150 cm^{-1} to 2500 cm^{-1} , Fig. 4c plots the fitted polaritonic dephasing rate (magenta squares for the UP and cyan circles for the LP) versus the cavity mode detuning from nonequilibrium CavMD simulations after a weak, resonant pumping of the corresponding polaritons. Similar to Fig. 4b, here we also compare the fitted rate to $\alpha|X_{\pm}^{(B)}|^2 J_{\pm}$ (where $\alpha = 1200 \text{ ps}^{-1}/\text{cm}$ is set the same as Fig. 4b), which is calculated from the linear IR spectra inside versus outside the cavity (see Eq. (23)). Note that the IR spectra for a detuned cavity mode has been plotted in Ref.⁴⁵ and is not given here.

As shown in Fig. 4c, the two results agree well for the UP (magenta squares). For the LP, there is a modest underestimation of $\alpha|X_{\pm}^{(B)}|^2 J_{\pm}$ compared with the fitted dephasing rate (cyan circles) when the cavity mode detuning is near zero, which corresponds to the LP frequency ($\sim 2241 \text{ cm}^{-1}$) where polariton enhanced molecular nonlinear absorption occurs. Interestingly, when the cavity mode is very positively detuned, the fitted dephasing rate becomes slightly smaller than $\alpha|X_{\pm}^{(B)}|^2 J_{\pm}$, where we expect that the two results agree with each other (since the nonlinear absorption mechanism should vanish when the LP frequency becomes closer to the fundamental vibrational frequency). For the moment, there is no obvious explanation for this disagreement. Because the fitted dephasing rate is very large when the cavity mode is very positively detuned, an error in numerical fitting can not be entirely ruled out.

3. Molecular density dependence

The Rabi splitting and cavity mode detuning studies have shown that the fitted polaritonic dephasing rate agrees with $|X_{\pm}^{(B)}|^2 J_{\pm}$ very well if polariton-enhanced molecular nonlinear mechanism does not play an important role. In order to fully validate the agreement between CavMD and the FGR rate in Eq. (16), we further examine the correlation between intermolecular interactions (Δ) and the polaritonic dephasing rate. Figs. 2 and 3 have shown such an example: by decreasing intermolecular interactions (via reducing the molecular density), both the UP and LP lifetimes become longer.

Fig. 5 shows more comprehensive data examining how the polariton decay rate ($1/\tau_{\pm}$) depends on molecular density (under a fixed Rabi splitting). When the cavity mode frequency is $\omega_c = 2320 \text{ cm}^{-1}$ and the effective light-matter coupling is $\tilde{\varepsilon} = 2 \times 10^{-4} \text{ a.u.}$, Fig. 5a shows that both the fitted UP and LP dephasing rates increase when the molecular density increases. Moreover, this dependence appears to be linear. Note that as shown in the inset of Fig. 3a, since changing the molecular density can slightly modify the lineshapes (while keeping the Rabi splitting constant), the spectral overlap J_{\pm} is also a function of the molecular density. In order to exclude the influence of J_{\pm} , in Fig. 5b we plot the corresponding $1/\tau_{\pm} J_{\pm}$ versus the molecular density. Again, $1/\tau_{\pm} J_{\pm}$ increases when the molecular density increases. This dependence highlights the fact that it is intermolecular interactions which control the polariton dephasing rate under a weak external excitation; this conclusion is consistent with the premise of the FGR rate in Eq. (16), although the linear dependence on the density no longer holds for the UP.

4. Molecular system size dependence

There is a piece of hidden information in Eq. (16): the polaritonic dephasing rate should be independent of the molecular number — provided the Rabi splitting, cavity mode frequency, and molecular density are the same. In Ref.⁴⁵ (see Fig. 7 therein), we have reported that the CavMD polariton dephasing rate shows this independence for both the LP and the UP.

IV. CONCLUSION

In conclusion, we have extensively studied the parameter dependence (including the cavity loss, Rabi splitting, cavity mode detuning, and molecular density) of the polariton relaxation lifetime with nonequilibrium CavMD simulations when the polariton is excited with a weak laser pulse. By comparing the simulation results with a FGR rate from a tight-binding harmonic model, we find a very good agreement for the UP lifetime and sometimes a modest disagreement for the LP. Such a disagreement does not void the validity of CavMD. By contrast, it is an

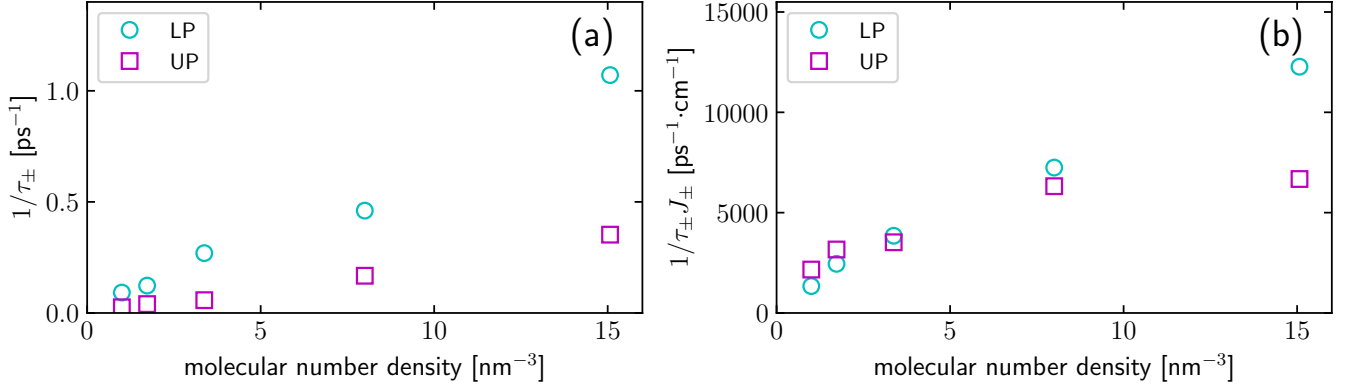


FIG. 5. (a) Polariton decay rate ($1/\tau_{\pm}$) versus the molecular number density when $\omega_c = 2320 \text{ cm}^{-1}$ and $\tilde{\varepsilon} = 2 \times 10^{-4} \text{ a.u.}$. Here, the molecular density is changed by tuning the simulation cell length while keeping the molecular number the same (so the Rabi splitting is fixed). See Sec. II B 1 for other simulation details. (b) The corresponding $1/\tau_{\pm}J_{\pm}$ versus the molecular number density.

indicator of the incompleteness of the quantum model we use: this model does not consider molecular anharmonicity and high excited states of vibrations, so this model fails to capture polariton enhanced molecular nonlinear absorption^{44,45}, an important mechanism which can also alter the relaxation of the polaritons.

In fact, the agreement between nonequilibrium CavMD simulations and the FGR rate is not surprising: on the one hand, classical molecular dynamics simulations can often describe molecular vibrational relaxation outside the cavity even for the high frequency vibrations^{69–71}; on the other hand, in the area of light-matter interactions, classical theory has been shown to agree with quantum FGR rates very well (at least as far as parameter dependence), e.g., the spontaneous emission rate inside⁷⁸ or outside^{79,80} a cavity. Hence, by inheriting the both sides, CavMD is expected to deal with many VSC dynamics reasonably well.

As far as the polariton relaxation mechanism is considered, our simulation indicates that since the polariton inherits the photonic character only partially and the formation of Rabi splitting separates the lineshapes between molecular bright and dark modes, the polariton lifetime can be longer than both the cavity lifetime and the bright-mode dephasing lifetime outside the cavity (where the bright and dark modes are degenerate and the dephasing rate should be very large). Thus, polaritons (especially the UP) may exhibit a more long-lived coherence than either the cavity photon or the molecular subsystem²⁸, demonstrating the benefits of forming strong light-matter interactions. By designing cavities with a high Q factor (or small loss) and a very large Rabi splitting, it is possible to create molecular polaritons which could survive for a very long time before relaxation. Such long-lived molecular polaritons might be a good platform for quantum information applications in the future.

Appendix S-I THE PULSE PROFILE

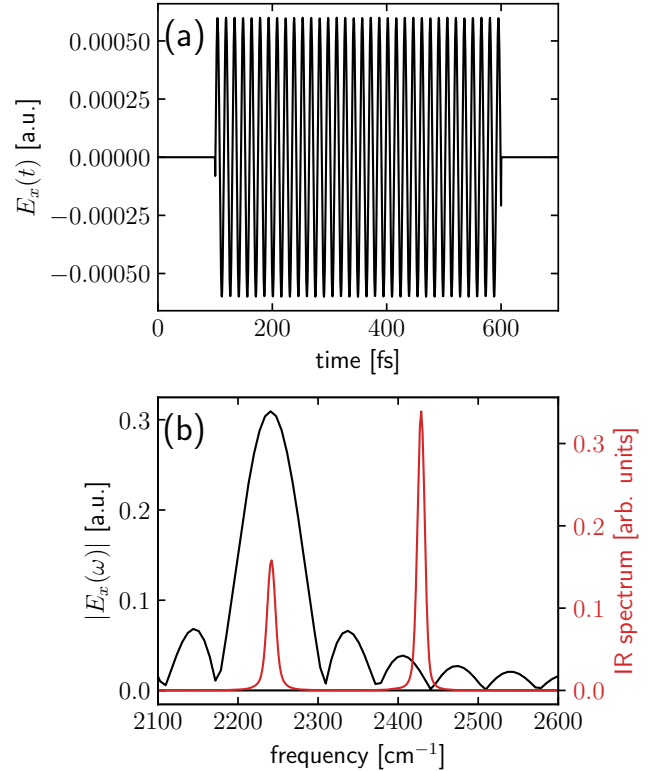


FIG. 6. (a) The E-field profile $E_x(t)$ defined in Eq. (21), where the pulse frequency is set as the LP frequency of Fig. 2: $\omega = \omega_{\text{LP}} = 2241 \text{ cm}^{-1}$. (b) The corresponding E-field spectrum in the frequency domain. The red line replots the Rabi splitting spectrum in the inset of Fig. 2a.

Appendix S-II NONADDITIVE EFFECTS IN POLARITONIC DECAY RATES

Polaritons are hybrid light-matter states, so one might naively think that a polaritonic property is a linear combination of the photonic contribution (with a weight $|X_{\pm}^{(c)}|^2$) plus the molecular bright-mode contribution (with a weight $|X_{\pm}^{(B)}|^2$). For example, for the polaritonic decay rate under VSC, if one applies Eq. (9), one can simply obtain:

$$\frac{\partial(1/\tau_{\pm})}{\partial k_c} = |X_{\pm}^{(c)}|^2 \quad (\text{S1a})$$

$$\frac{\partial(1/\tau_{\pm})}{\partial k_B} = |X_{\pm}^{(B)}|^2 \quad (\text{S1b})$$

In this work, we have found the importance of the polaritonic dephasing rate (γ_{\pm}) on the polaritonic decay rate. According to Eqs. (15) and (16), since γ_{\pm} is a complicated function of k_c , k_B , and the Rabi splitting, we find that

$$\frac{\partial(1/\tau_{\pm})}{\partial k_c} = |X_{\pm}^{(c)}|^2 + \frac{\partial\gamma_{\pm}}{\partial k_c} \neq |X_{\pm}^{(c)}|^2 \quad (\text{S2a})$$

$$\frac{\partial(1/\tau_{\pm})}{\partial k_B} = |X_{\pm}^{(B)}|^2 + \frac{\partial\gamma_{\pm}}{\partial k_B} \neq |X_{\pm}^{(B)}|^2 \quad (\text{S2b})$$

This equation implies that the simple additive feature no longer holds when the polaritonic dephasing rate is large. For example, increasing the cavity loss rate k_c can broaden the polaritonic lineshape and alter the spectral overlap between the polaritons and dark modes, leading to modified γ_{\pm} . Similarly, changing k_B can simultaneously alter the polaritonic and dark-mode lineshapes, which can also influence γ_{\pm} . In Fig. 2c, we have shown that $\partial(1/\tau_{-})/\partial k_c \neq |X_{\pm}^{(c)}|^2$ for liquid CO_2 under VSC.

- ¹J. Flick, M. Ruggenthaler, H. Appel, and A. Rubio, "Atoms and Molecules in Cavities, from Weak to Strong Coupling in Quantum-Electrodynamics (QED) Chemistry," *Proc. Natl. Acad. Sci. U.S.A.* **114**, 3026–3034 (2017).
- ²R. F. Ribeiro, L. A. Martínez-Martínez, M. Du, J. Campos-Gonzalez-Angulo, and J. Yuen-Zhou, "Polariton Chemistry: Controlling Molecular Dynamics with Optical Cavities," *Chem. Sci.* **9**, 6325–6339 (2018).
- ³J. Flick, N. Rivera, and P. Narang, "Strong Light-matter Coupling in Quantum Chemistry and Quantum Photonics," *Nanophotonics* **7**, 1479–1501 (2018).
- ⁴F. Herrera and J. Owrutsky, "Molecular polaritons for controlling chemistry with quantum optics," *J. Chem. Phys.* **152**, 100902 (2020).
- ⁵K. Hirai, J. A. Hutchison, and H. Uji-i, "Recent Progress in Vibropolaritonic Chemistry," *Chempluschem* **85**, 1981–1988 (2020).
- ⁶C. Climent, F. J. Garcia-Vidal, and J. Feist, "CHAPTER 10. Cavity-modified Chemistry: Towards Vacuum-field Catalysis," (Royal Society of Chemistry, 2021) pp. 343–393.
- ⁷B. Xiang and W. Xiong, "Molecular Vibrational Polariton: Its Dynamics and Potentials in Novel Chemistry and Quantum Technology," *J. Chem. Phys.* **155**, 050901 (2021).
- ⁸F. J. Garcia-Vidal, C. Ciuti, and T. W. Ebbesen, "Manipulating Matter by Strong Coupling to Vacuum Fields," *Science* **373**, eabd0336 (2021).
- ⁹A. Shalabney, J. George, H. Hiura, J. A. Hutchison, C. Genet, P. Hellwig, and T. W. Ebbesen, "Enhanced Raman Scattering from Vibro-Polariton Hybrid States," *Angew. Chemie* **127**, 8082–8086 (2015).

- ¹⁰J. P. Long and B. S. Simpkins, "Coherent Coupling between a Molecular Vibration and Fabry–Pérot Optical Cavity to Give Hybridized States in the Strong Coupling Limit," *ACS Photonics* **2**, 130–136 (2015).
- ¹¹B. S. Simpkins, K. P. Fears, W. J. Dressick, B. T. Spann, A. D. Dunkelberger, and J. C. Owrutsky, "Spanning Strong to Weak Normal Mode Coupling between Vibrational and Fabry–Pérot Cavity Modes through Tuning of Vibrational Absorption Strength," *ACS Photonics* **2**, 1460–1467 (2015).
- ¹²J. George, A. Shalabney, J. A. Hutchison, C. Genet, and T. W. Ebbesen, "Liquid-Phase Vibrational Strong Coupling," *J. Phys. Chem. Lett.* **6**, 1027–1031 (2015).
- ¹³A. Thomas, J. George, A. Shalabney, M. Dryzhakov, S. J. Varma, J. Moran, T. Chervy, X. Zhong, E. Devaux, C. Genet, J. A. Hutchison, and T. W. Ebbesen, "Ground-State Chemical Reactivity under Vibrational Coupling to the Vacuum Electromagnetic Field," *Angew. Chemie Int. Ed.* **55**, 11462–11466 (2016).
- ¹⁴R. M. A. Vergauwe, A. Thomas, K. Nagarajan, A. Shalabney, J. George, T. Chervy, M. Seidel, E. Devaux, V. Torbeev, and T. W. Ebbesen, "Modification of Enzyme Activity by Vibrational Strong Coupling of Water," *Angew. Chemie Int. Ed.* **58**, 15324–15328 (2019).
- ¹⁵A. Thomas, A. Jayachandran, L. Lethuillier-Karl, R. M. Vergauwe, K. Nagarajan, E. Devaux, C. Genet, J. Moran, and T. W. Ebbesen, "Ground State Chemistry under Vibrational Strong Coupling: Dependence of Thermodynamic Parameters on the Rabi Splitting Energy," *Nanophotonics* **9**, 249–255 (2020).
- ¹⁶A. Thomas, L. Lethuillier-Karl, K. Nagarajan, R. M. A. Vergauwe, J. George, T. Chervy, A. Shalabney, E. Devaux, C. Genet, J. Moran, and T. W. Ebbesen, "Tilting a Ground-State Reactivity Landscape by Vibrational Strong Coupling," *Science* **363**, 615–619 (2019).
- ¹⁷J. Lather, P. Bhatt, A. Thomas, T. W. Ebbesen, and J. George, "Cavity Catalysis by Cooperative Vibrational Strong Coupling of Reactant and Solvent Molecules," *Angew. Chemie Int. Ed.* **58**, 10635–10638 (2019).
- ¹⁸Y. Pang, A. Thomas, K. Nagarajan, R. M. A. Vergauwe, K. Joseph, B. Patraha, K. Wang, C. Genet, and T. W. Ebbesen, "On the Role of Symmetry in Vibrational Strong Coupling: The Case of Charge-Transfer Complexation," *Angew. Chemie Int. Ed.* **59**, 10436–10440 (2020).
- ¹⁹A. Sau, K. Nagarajan, B. Patraha, L. Lethuillier-Karl, R. M. A. Vergauwe, A. Thomas, J. Moran, C. Genet, and T. W. Ebbesen, "Modifying Woodward–Hoffmann Stereoselectivity Under Vibrational Strong Coupling," *Angew. Chemie* **133**, 5776–5781 (2021).
- ²⁰J. Lather and J. George, "Improving Enzyme Catalytic Efficiency by Co-operative Vibrational Strong Coupling of Water," *J. Phys. Chem. Lett.* **12**, 379–384 (2021).
- ²¹K. Hirai, H. Ishikawa, T. Chervy, J. A. Hutchison, and H. Uji-i, "Selective Crystallization via Vibrational Strong Coupling," *Chem. Sci.* (2021), 10.1039/D1SC03706D.
- ²²A. D. Dunkelberger, B. T. Spann, K. P. Fears, B. S. Simpkins, and J. C. Owrutsky, "Modified Relaxation Dynamics and Coherent Energy Exchange in Coupled Vibration-Cavity Polaritons," *Nat. Commun.* **7**, 1–10 (2016).
- ²³A. D. Dunkelberger, R. B. Davidson, W. Ahn, B. S. Simpkins, and J. C. Owrutsky, "Ultrafast Transmission Modulation and Recovery via Vibrational Strong Coupling," *J. Phys. Chem. A* **122**, 965–971 (2018).
- ²⁴B. Xiang, R. F. Ribeiro, A. D. Dunkelberger, J. Wang, Y. Li, B. S. Simpkins, J. C. Owrutsky, J. Yuen-Zhou, and W. Xiong, "Two-dimensional infrared spectroscopy of vibrational polaritons," *Proc. Natl. Acad. Sci. U.S.A.* **115**, 4845–4850 (2018).
- ²⁵B. Xiang, R. F. Ribeiro, Y. Li, A. D. Dunkelberger, B. B. Simpkins, J. Yuen-Zhou, and W. Xiong, "Manipulating Optical Nonlinearities of Molecular Polaritons by Delocalization," *Sci. Adv.* **5**, eaax5196 (2019).
- ²⁶B. Xiang, R. F. Ribeiro, L. Chen, J. Wang, M. Du, J. Yuen-Zhou, and W. Xiong, "State-Selective Polariton to Dark State Relaxation Dynamics," *J. Phys. Chem. A* **123**, 5918–5927 (2019).
- ²⁷B. Xiang, R. F. Ribeiro, M. Du, L. Chen, Z. Yang, J. Wang, J. Yuen-Zhou, and W. Xiong, "Intermolecular Vibrational En-

- ergy Transfer Enabled by Microcavity Strong Light–Matter Coupling,” *Science* **368**, 665–667 (2020).
- ²⁸A. B. Grafton, A. D. Dunkelberger, B. S. Simpkins, J. F. Triana, F. J. Hernández, F. Herrera, and J. C. Owrutsky, “Excited-State Vibration-Polariton Transitions and Dynamics in Nitroprusside,” *Nat. Commun.* **12**, 214 (2021).
 - ²⁹B. Xiang, J. Wang, Z. Yang, and W. Xiong, “Nonlinear Infrared Polaritonic Interaction between Cavities Mediated by Molecular Vibrations at Ultrafast Time Scale,” *Sci. Adv.* **7**, eabf6397 (2021).
 - ³⁰J. Galego, C. Climent, F. J. Garcia-Vidal, and J. Feist, “Cavity Casimir-Polder Forces and Their Effects in Ground-State Chemical Reactivity,” *Phys. Rev. X* **9**, 021057 (2019).
 - ³¹J. A. Campos-Gonzalez-Angulo, R. F. Ribeiro, and J. Yuen-Zhou, “Resonant Catalysis of Thermally Activated Chemical Reactions with Vibrational Polaritons,” *Nat. Commun.* **10**, 4685 (2019).
 - ³²T. E. Li, A. Nitzan, and J. E. Subotnik, “On the Origin of Ground-State Vacuum-Field Catalysis: Equilibrium Consideration,” *J. Chem. Phys.* **152**, 234107 (2020).
 - ³³J. A. Campos-Gonzalez-Angulo and J. Yuen-Zhou, “Polaritonic normal modes in transition state theory,” *J. Chem. Phys.* **152**, 161101 (2020).
 - ³⁴X. Li, A. Mandal, and P. Huo, “Cavity frequency-dependent theory for vibrational polariton chemistry,” *Nat. Commun.* **12**, 1315 (2021).
 - ³⁵C. Climent and J. Feist, “On the S N 2 reactions modified in vibrational strong coupling experiments: reaction mechanisms and vibrational mode assignments,” *Phys. Chem. Chem. Phys.* **22**, 23545–23552 (2020).
 - ³⁶D. Sidler, C. Schäfer, M. Ruggenthaler, and A. Rubio, “Polaritonic Chemistry: Collective Strong Coupling Implies Strong Local Modification of Chemical Properties,” *J. Phys. Chem. Lett.* **12**, 508–516 (2021).
 - ³⁷M. Du, J. A. Campos-Gonzalez-Angulo, and J. Yuen-Zhou, “Nonequilibrium effects of cavity leakage and vibrational dissipation in thermally activated polariton chemistry,” *J. Chem. Phys.* **154**, 084108 (2021).
 - ³⁸C. Schäfer, J. Flick, E. Ronca, P. Narang, and A. Rubio, “Shining Light on the Microscopic Resonant Mechanism Responsible for Cavity-Mediated Chemical Reactivity,” (2021), arXiv:2104.12429.
 - ³⁹J. D. Pino, J. Feist, and F. J. Garcia-Vidal, “Quantum theory of collective strong coupling of molecular vibrations with a microcavity mode,” *New J. Phys.* **17**, 053040 (2015).
 - ⁴⁰P. Saurabh and S. Mukamel, “Two-dimensional Infrared Spectroscopy of Vibrational Polaritons of Molecules in an Optical Cavity,” *J. Chem. Phys.* **144**, 124115 (2016).
 - ⁴¹R. F. Ribeiro, A. D. Dunkelberger, B. Xiang, W. Xiong, B. S. Simpkins, J. C. Owrutsky, and J. Yuen-Zhou, “Theory for Nonlinear Spectroscopy of Vibrational Polaritons,” *J. Phys. Chem. Lett.* **9**, 3766–3771 (2018).
 - ⁴²M. Du, L. A. Martínez-Martínez, R. F. Ribeiro, Z. Hu, V. M. Menon, and J. Yuen-Zhou, “Theory for polariton-assisted remote energy transfer,” *Chem. Sci.* **9**, 6659–6669 (2018).
 - ⁴³Z. Zhang, K. Wang, Z. Yi, M. S. Zubairy, M. O. Scully, and S. Mukamel, “Polariton-Assisted Cooperativity of Molecules in Microcavities Monitored by Two-Dimensional Infrared Spectroscopy,” *J. Phys. Chem. Lett.* **10**, 4448–4454 (2019).
 - ⁴⁴R. F. Ribeiro, J. A. Campos-Gonzalez-Angulo, N. C. Giebink, W. Xiong, and J. Yuen-Zhou, “Enhanced optical nonlinearities under collective strong light-matter coupling,” *Phys. Rev. A* **103**, 063111 (2021).
 - ⁴⁵T. E. Li, A. Nitzan, and J. E. Subotnik, “Cavity molecular dynamics simulations of vibrational polariton-enhanced molecular nonlinear absorption,” *J. Chem. Phys.* **154**, 094124 (2021).
 - ⁴⁶R. Sáez-Blázquez, J. Feist, A. I. Fernández-Domínguez, and F. J. García-Vidal, “Organic polaritons enable local vibrations to drive long-range energy transfer,” *Phys. Rev. B* **97**, 241407 (2018).
 - ⁴⁷C. Sommer, M. Reitz, F. Mineo, and C. Genes, “Molecular polaritonics in dense mesoscopic disordered ensembles,” *Phys. Rev. Res.* **3**, 033141 (2021).
 - ⁴⁸H. L. Luk, J. Feist, J. J. Toppari, and G. Groenhof, “Multiscale Molecular Dynamics Simulations of Polaritonic Chemistry,” *J. Chem. Theory Comput.* **13**, 4324–4335 (2017).
 - ⁴⁹G. Groenhof, C. Climent, J. Feist, D. Morozov, and J. J. Toppari, “Tracking Polariton Relaxation with Multiscale Molecular Dynamics Simulations,” *J. Phys. Chem. Lett.* **10**, 5476–5483 (2019).
 - ⁵⁰R. H. Tichauer, J. Feist, and G. Groenhof, “Multi-scale dynamics simulations of molecular polaritons: The effect of multiple cavity modes on polariton relaxation,” *J. Chem. Phys.* **154**, 104112 (2021).
 - ⁵¹J. F. Triana, F. J. Hernández, and F. Herrera, “The shape of the electric dipole function determines the sub-picosecond dynamics of anharmonic vibrational polaritons,” *J. Chem. Phys.* **152**, 234111 (2020).
 - ⁵²T. E. Li, J. E. Subotnik, and A. Nitzan, “Cavity molecular dynamics simulations of liquid water under vibrational ultrastrong coupling,” *Proc. Natl. Acad. Sci. U.S.A* **117**, 18324–18331 (2020).
 - ⁵³T. E. Li, A. Nitzan, and J. E. Subotnik, “Collective Vibrational Strong Coupling Effects on Molecular Vibrational Relaxation and Energy Transfer: Numerical Insights via Cavity Molecular Dynamics Simulations,” *Angew. Chemie Int. Ed.* **60**, 15533–15540 (2021).
 - ⁵⁴T. E. Li, A. Nitzan, and J. E. Subotnik, “Energy-efficient pathway for selectively exciting solute molecules to high vibrational states via solvent vibration-polariton pumping,” arXiv , 2104.15121 (2021), arXiv:2104.15121.
 - ⁵⁵M. Tavis and F. W. Cummings, “Exact Solution for an N-Molecule–Radiation-Field Hamiltonian,” *Phys. Rev.* **170**, 379–384 (1968).
 - ⁵⁶M. Tavis and F. W. Cummings, “Approximate Solutions for an N-Molecule–Radiation-Field Hamiltonian,” *Phys. Rev.* **188**, 692–695 (1969).
 - ⁵⁷S. Rudin and T. L. Reinecke, “Oscillator model for vacuum Rabi splitting in microcavities,” *Phys. Rev. B* **59**, 10227–10233 (1999).
 - ⁵⁸A. Junginger, F. Wackenhut, A. Stuhl, F. Blendinger, M. Brecht, and A. J. Meixner, “Tunable strong coupling of two adjacent optical $\lambda/2$ Fabry-Pérot microresonators,” *Opt. Express* **28**, 485 (2020).
 - ⁵⁹O. Di Stefano, A. Settineri, V. Macrì, L. Garziano, R. Stassi, S. Savasta, and F. Nori, “Resolution of gauge ambiguities in ultrastrong-coupling cavity quantum electrodynamics,” *Nat. Phys.* **15**, 803–808 (2019).
 - ⁶⁰C. Schäfer, M. Ruggenthaler, V. Rokaž, and A. Rubio, “Relevance of the Quadratic Diamagnetic and Self-Polarization Terms in Cavity Quantum Electrodynamics,” *ACS Photonics* **7**, 975–990 (2020).
 - ⁶¹M. A. D. Taylor, A. Mandal, W. Zhou, and P. Huo, “Resolution of Gauge Ambiguities in Molecular Cavity Quantum Electrodynamics,” *Phys. Rev. Lett.* **125**, 123602 (2020).
 - ⁶²R. Houdré, R. P. Stanley, and M. Ilegems, “Vacuum-field Rabi splitting in the presence of inhomogeneous broadening: Resolution of a homogeneous linewidth in an inhomogeneously broadened system,” *Phys. Rev. A* **53**, 2711–2715 (1996).
 - ⁶³H. Deng, H. Haug, and Y. Yamamoto, “Exciton-polariton Bose-Einstein condensation,” *Rev. Mod. Phys.* **82**, 1489–1537 (2010).
 - ⁶⁴Note that this expression is valid only when Rabi splitting is larger than the linewidth of either the photonic or molecular peak.
 - ⁶⁵When considering the radiative relaxation of k_B , we also disregard the possibility that collective radiative emission can be faster than single molecule emission and also the Purcell effect.
 - ⁶⁶T. Förster, “Zwischenmolekulare Energiewanderung und Fluoreszenz,” *Ann. Phys.* **437**, 55–75 (1948).
 - ⁶⁷Of course, γ_{\pm} is also a function of the Rabi splitting.
 - ⁶⁸G. R. Medders and F. Paesani, “Infrared and Raman Spectroscopy of Liquid Water through “First-Principles” Many-Body Molecular Dynamics,” *J. Chem. Theory Comput.* **11**, 1145–1154 (2015).
 - ⁶⁹C. Heidebach, I. I. Fedchenia, D. Schwarzer, and J. Schroeder, “Molecular-dynamics simulation of collisional energy transfer from vibrationally highly excited azulene in compressed CO₂,” *J. Chem. Phys.* **108**, 10152–10161 (1998).
 - ⁷⁰V. N. Kabadi and B. M. Rice, “Molecular Dynamics Simula-

- tions of Normal Mode Vibrational Energy Transfer in Liquid Nitromethane,” *J. Phys. Chem. A* **108**, 532–540 (2004).
- ⁷¹A. Kandratsenka, J. Schroeder, D. Schwarzer, and V. S. Vikhrenko, “Nonequilibrium molecular dynamics simulations of vibrational energy relaxation of HOD in D₂O,” *J. Chem. Phys.* **130**, 174507 (2009).
- ⁷²R. T. Cygan, V. N. Romanov, and E. M. Myshakin, “Molecular Simulation of Carbon Dioxide Capture by Montmorillonite Using an Accurate and Flexible Force Field,” *J. Phys. Chem. C* **116**, 13079–13091 (2012).
- ⁷³D. A. McQuarrie, *Statistical Mechanics* (Harper-Collins Publishers, New York, 1976).
- ⁷⁴M.-P. Gaigeot and M. Sprik, “Ab Initio Molecular Dynamics Computation of the Infrared Spectrum of Aqueous Uracil,” *J. Phys. Chem. B* **107**, 10344–10358 (2003).
- ⁷⁵S. Habershon, D. E. Manolopoulos, T. E. Markland, and T. F. Miller, “Ring-Polymer Molecular Dynamics: Quantum Effects in Chemical Dynamics from Classical Trajectories in an Extended Phase Space,” *Annu. Rev. Phys. Chem.* **64**, 387–413 (2013).
- ⁷⁶A. Nitzan, *Chemical Dynamics in Condensed Phases: Relaxation, Transfer and Reactions in Condensed Molecular Systems* (Oxford University Press, New York, 2006).
- ⁷⁷T. Seki, J.-D. Grunwaldt, and A. Baiker, “In Situ Attenuated Total Reflection Infrared Spectroscopy of Imidazolium-Based Room-Temperature Ionic Liquids under “Supercritical” CO₂,” *J. Phys. Chem. B* **113**, 114–122 (2009).
- ⁷⁸A. E. Krasnok, A. P. Slobozhanyuk, C. R. Simovski, S. A. Tretyakov, A. N. Poddubny, A. E. Miroshnichenko, Y. S. Kivshar, and P. A. Belov, “An antenna model for the Purcell effect,” *Sci. Rep.* **5**, 12956 (2015).
- ⁷⁹J. D. Jackson, *Classical Electrodynamics*, 3rd ed. (John Wiley & Sons, New York, 1999).
- ⁸⁰W. H. Miller, “A Classical/Semiclassical Theory for the Interaction of Infrared Radiation with Molecular Systems,” *J. Chem. Phys.* **69**, 2188–2195 (1978).